Author's Accepted Manuscript

www.elsevier.com/locate/talanta

Nanoparticle based simple electrochemical biosensor platform for profiling of protein-nucleic acid interactions

Yifan Dai, Liang-Yuan Chiu, Yongkun Sui, Quanbin Dai, Srinivasa Penumutchu, Niyati Jain, Liming Dai, Christian A. Zorman, Blanton S. Tolbert, R. Mohan Sankaran, Chung Chiun Liu

PII: S0039-9140(18)31172-X
DOI: https://doi.org/10.1016/j.talanta.2018.11.021
Reference: TAL19254

To appear in: *Talanta*

Received date: 20 September 2018
Revised date: 2 November 2018
Accepted date: 5 November 2018

Cite this article as: Yifan Dai, Liang-Yuan Chiu, Yongkun Sui, Quanbin Dai, Srinivasa Penumutchu, Niyati Jain, Liming Dai, Christian A. Zorman, Blanton S. Tolbert, R. Mohan Sankaran and Chung Chiun Liu, Nanoparticle based simple electrochemical biosensor platform for profiling of protein-nucleic acid interactions, *Talanta,* https://doi.org/10.1016/j.talanta.2018.11.021

Nanoparticle based simple electrochemical biosensor platform for profiling of protein-nucleic acid interactions

Yifan Dai[a,b1], Liang-Yuan Chiu[c,1], Yongkun Sui[d], Quanbin Dai[e], Srinivasa Penumutchu[c], Niyati Jain[c], Liming Dai[e], Christian A. Zorman[d], Blanton S. Tolbert[c], R. Mohan Sankaran[a], Chung Chiun Liu[a,b*]

[a]Department of Chemical and Biomolecular Engineering, Case Western Reserve University, Cleveland, Ohio 44106, USA

[b]Electronics Design Center, Case Western Reserve University, Cleveland, Ohio 44106, USA

[c]Department of Chemistry, Case Western Reserve University, Cleveland, Ohio 44106, USA

[d]Electrical Engineering & Computer Science, Case Western Reserve University, Cleveland, Ohio 44106, USA

[e]Department of Macromolecular Science and Engineering, Case Western Reserve University, Cleveland, Ohio 44106, USA

*Corresponding Author

Abstract:

The analysis of protein-nucleic acid interactions is essential for biophysics related research. However, simple, rapid, and accurate methods for biomolecules interaction analysis are lacking. We herein establish an electrochemical biosensor approach for protein-nucleic acid binding analysis. The fabrication method of a highly-controlled, inkjet printing and plasma based nanoparticle sensor is presented. A novel bioconjugation method is demonstrated as a simple and rapid approach for protein-based biosensor fabrication. As a proof of concept, we analyzed the binding interaction between unwinding protein 1 (UP1) and SL3^{ESS3} RNA, confirming the accuracy of this nanoparticle based electrochemical biosensor approach with traditional biophysical methods. We further accurately profiled and differentiated a unique binding interaction pattern of multiple G-tract nucleic acid sequences with heterogeneous nuclear ribonucleoprotein H1. Our study provides insights into a potential universal platform for in vitro biomolecule interaction analysis based on an electrochemical biosensor approach.

Graphical abstract

[1] These authors contributed equally.

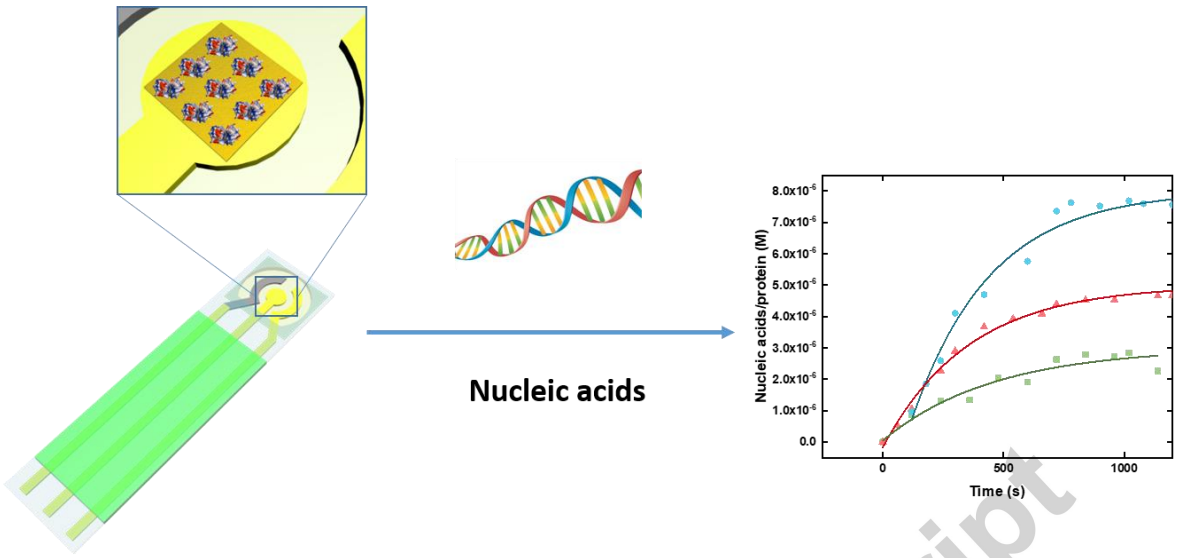

Keywords: microsystem for binding interaction analysis. plasma. nanoparticle electrochemical biosensor. heterogeneous nuclear ribonucleoprotein H1. G-tract nucleic acid.

1. Introduction

Quantitative sensing of biomolecules interactions is critical to fundamental understanding of biological pathways, biomarker analysis, drug function evaluation and biophysical properties study [1-8]. A cost-effective, sensitive, and biologically specific analytical technique combined with an accurate quantification model is desirable for these applications. Magnetically responsive nano-sensor demonstrated an accurate, high-throughput binding kinetic analysis method[6]. Silicon nano-wire field-effect transistors were also applied for the analysis of protein-ligand binding affinities[4]. These methods typically required complex fabricated sensing platform and expensive transduction mechanism. Therefore, these methods are not ideal for common laboratory arrangement. In order to develop this demanding analytical technique, we herein apply a nano-particle based highly sensitive universal biosensor platform as a powerful tool to quantify biomolecule interaction. This unique biosensor platform demonstrates a simple nanostructured electrode fabrication method based on plasma treatment and a novel universal biosensor fabrication process using a simple and rapid bioconjugation method. In this study, we apply this electrochemical biosensor platform to profile and distinguish the exclusive interaction pattern of multiple G-tract nucleic acid sequences with heterogeneous nuclear ribonucleoprotein H1 (hnRNP H1)[9-11].

A high-sensitivity and low-detection limit biosensor application typically requires a large sensing surface area based on nanoparticle covered electrode[12, 13]. Typically, researchers applied nanoparticle ink printing on different substrates with the assistance of organic capping molecules for the immobilization of nanoparticles, which significantly decreased the electric conductivity on the substrate surface[14]. Therefore, it is not ideal for high-sensitivity sensing applications. We herein present a unique and highly-controlled nanoparticle biosensor fabrication approach that uses inkjet printing with a post-print plasma treatment creating conductive gold nanoparticles (AuNPs) electrode from a metal (gold based) salt at ambient temperature.

In order to specifically recognize a target biomolecule in biosensor development, the immobilization of the biomolecule catalysts, such as enzyme, antibody and nucleic acid probe on the biosensor surface is required. Unfortunately, the common immobilization method, which often involves the use of self-assembled monolayer (SAM) to establish multifaceted organic layers for biomolecule bonding, which can significantly interfere with the selectivity and reproducibility of the biosensor[7, 15, 16]. Moreover, SAM requires complex surface treatment process that are time-consuming and exhibit a low-reproducibility [17-19]. In this study, we employed a single-layer system using bioconjugation chemistry for the immobilization of biomolecules for the biosensor fabrication[20], which considerably enhanced the time-efficiency for biosensor production. Furthermore, it simplified the alignment of the immobilized biomolecules on the biosensor surface, generating a highly sensitive and readily biomolecule accessible platform for biomolecule detection.

Quantification of nucleic acid is a powerful solution for the diagnosis of infectious diseases at a time-sensitive manner, mostly using enzymatic amplification strategy for nucleic acid sequence determination[21]. We hereby present a new perspective for nucleic acid sequence study using specific nucleotide binding protein along with the biosensor platform. Based on an accurate quantitative analysis using differential pulse voltammetry (DPV), further analysis of biophysical property of certain biomolecules, such as binding interaction, can be accomplished. DPV provides a direct electrochemical quantification of biomolecule complexes on the biosensor surface, and is therefore free of enzymatic amplification bias[7, 22]. In this study, the quantification of nucleic acid-protein complexes was achieved by monitoring the Faradic current generated by $[Fe[CN]_6]^{3-/4-}$[23, 24], which was a negative correlated function of surface impedance produced by the quantity of immobilized nucleic acid-protein complexes. The obtained current signal was calibrated by Hill equation to compute the dissociation constant (K_D) [25]. The association rate (k_{on}) was also modeled based on the same concentration of nucleic acid solution versus different static incubation time. This technique demonstrated an accurate fit of the binding interaction models based on the concise experimental condition. Our investigations provide a new approach for quantification of biomolecule interaction, using electrochemical method along with rapid fabrication of AuNPs sensor. Using this high-sensitivity biosensing platform, we were able to distinguish the binding effect based on wild type hnRNP H1 protein with different nucleic acid oligomers.

2. Results and Discussion

2.1 Characterization of bioconjugation modified protein

In order to immobilize the target protein onto the gold electrode surface, bioconjugation method was applied to provide an external thiol linker onto the protein[26]. Figure 1A demonstrates the bioconjugation process of N-succinimidyl S-acetylthioacetate **(**SATA) and hnRNP H1 HqRRM12 (H12) protein. Comparing with the long processing time (over 48 hrs) of traditional SAM method, this immobilization procedure only takes 1hr to form a highly-aligned and simplified protein layer, which can then be further interacted with other biomolecules. We assessed the thiolation of the protein based on the bioconjugation method using Matrix Assisted Laser Desorption/Ionization (MALDI-TOF). As shown in Figure 1B, MALDI-TOF confirms the increase in the molar mass of the H12 protein after conjugation with SATA. The theoretical molecular weight of H12 without SATA modification is 21.271kDa. The average mass result of H12 with conjugated SATA was 21.369kDa, which was close to the addition of one SATA molecule. Moreover, a previous study has demonstrated that this external modification would not affect

the tertiary structure of the protein, therefore does not perturb the binding function of the domain.[26] This conjugated protein can then be stored at -20°C and ready for biosensor fabrication.

2.2 Characterization of plasma converted gold biosensor

We further characterized the nanoparticle-containing working electrode fabricated by inkjet printing and plasma treatment based on a three-electrode biosensor prototype (Figure 1), which was defined and characterized in previous studies[7, 26]. Gold was selected as the material because of its strong affinity with thiol group, providing a stable linkage with biomolecules[16]. The plasma converted AuNPs working electrode is shown in Figure 1C. XRD characterization of gold is shown in Figure 1D. Cyclic voltammetry was then used to assess the stability and reproducibility of the AuNPs sensor. Cyclic voltammograms (Figure 1E) were obtained at different scan rates ranging from 20mV/s to 120mV/s in a redox solution containing 5mM $[Fe(CN)_6]^{3-/4-}$ with 0.1 M KCl. According to Randles-Sevick equation[27], the square root of the scan rate was linearly proportional to the current (Figure 1F). The standard deviation based on n=3 was less than 1.5% and the R- square value was 0.99847, indicating a high reproducibility and stability. Also, comparing with chemical vapor deposition fabricated biosensor[7], the conductivity of the plasma-converted AuNPs biosensor was about 50% higher based on the current outputs from the cyclic voltammetry.

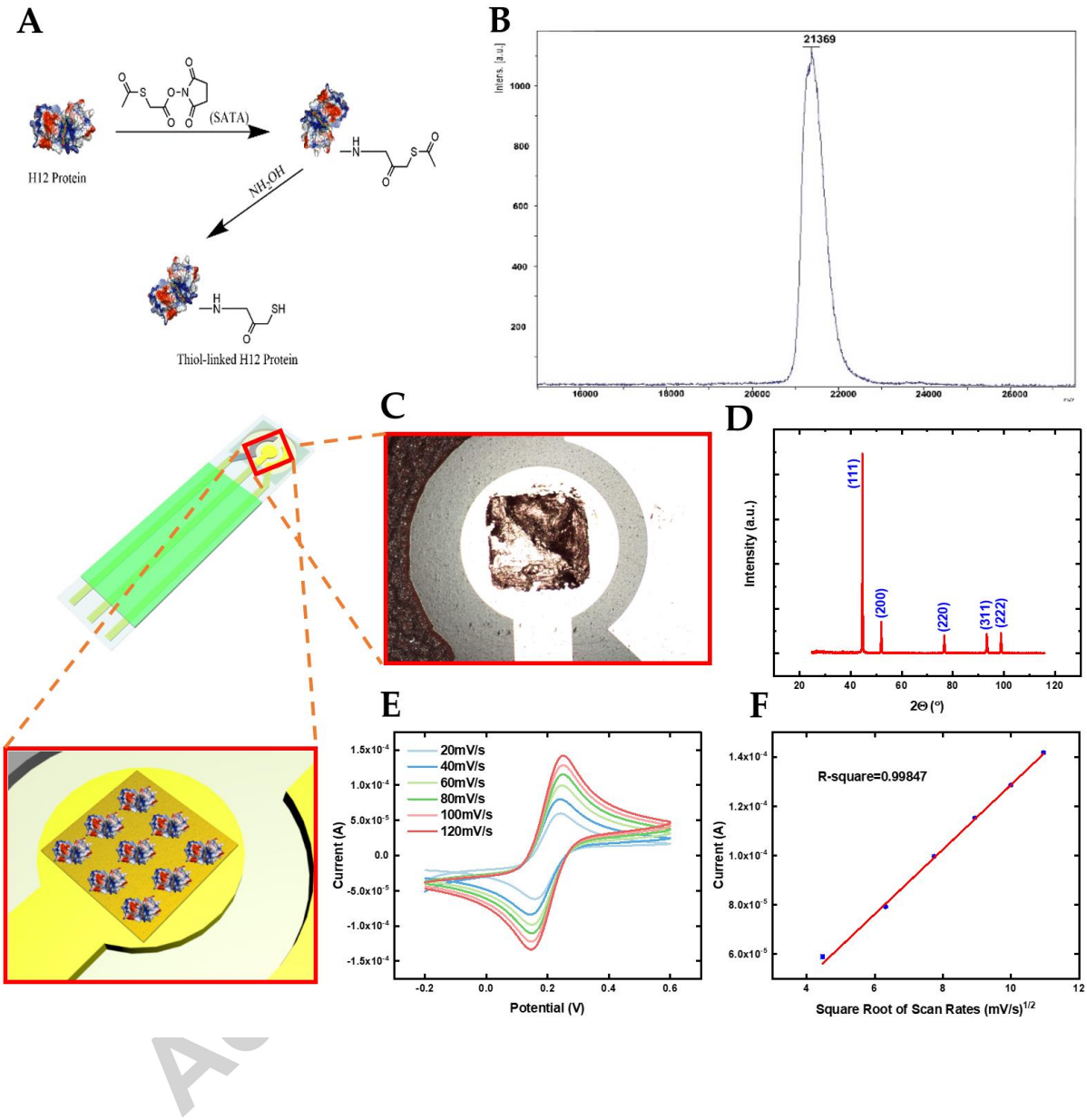

Figure 1. A) Bioconjugation reaction mechanism using N-succinimidyl S-acetylthioacetate (SATA) to produce thiol-linked hnRNP H1 protein. B) MALDI-TOF mass spectrum of HqRRM12 protein with one SATA labeling. A sample HqRRM12 intact spectrum is reported in the range between 10000 to 20000 m/z. C) Microscope picture of the AuNPs cluster on working electrode. Optical profilometry of the printed AuNPs. D) XRD characterization of plasma converted gold electrode. E) Cyclic voltammetry characterization of AuNPs sensor surface based on scan rate from 20mV/S- 120mV/s. F) Linear calibration plot based on oxidation current outputs from cyclic voltammetry against square root of scan rates.

2.3 Analysis of biosensor performance

As shown in section 2.2, plasma converted AuNPs biosensor shows a higher level of conductivity comparing with that of traditional chemical vapor deposited gold-based biosensor. Therefore, we further examine the morphology of plasma converted gold layer. The top-down SEM image of the AuNPs film (Figure 2A) shows that the printed Au has a Velcro-loop like morphology. Plasma treatment is a simply controlled metal conversion process by fixing the voltage and pressure[28], which provides a reproducible morphology based on inkjet printing. This highly-controlled process makes it suitable for fabrication of cost-effective single-use sensor. The root-mean-square (RMS) value of the surface roughness was 390 nm as calculated from the profilometry data shown in Figure 2B.

The morphology roughness of the plasma converted gold surface can contribute to a higher biomolecule accessibility, leading to improvements on the detection sensitivity and detection limit. Therefore, the biomolecule accessibility of the plasma converted AuNPs electrode was compared with the chemical vapor deposited Au electrode. Using the thiol-linked H12 protein, we assessed the amount of biomolecule tethered on the electrode based on the same incubation period. As shown in Figure 2C, plasma converted sensor shows a higher change of current outputs based on DPV measurements at the same incubation time comparing with that of vapor deposited sensor. This result indicated that a rougher electrode surface provides a higher degree of biomolecule accessibility and a faster biomolecule absorption process.

Time of Flight- Secondary Ions Mass spectroscopy (TOF-SIMS) was also used to further confirm the effectiveness of the reaction with the thiol-linked protein and the biomolecule accessibility difference based on these two types biosensors. Au-S bond mapping was obtained through TOF-SIMS analysis based on negative polarity. The sputtering gold electrode and plasma reduced AuNPs covered electrode were both applied for thiol-linked H12 protein incubation process for the same amount of time. As shown in Figure 2D, the plasma reduced gold nanoparticles covered electrode showed nearly 19 times higher Au-S bond counts comparing with that of the sputtering gold electrode, indicating that the AuNPs electrode possessed a much larger effective gold surface area available for the formation of gold-sulfur bond on the electrode surface. Combination of the above results confirmed and demonstrated two critical points of this biosensor development. First, effectiveness of bioconjugation chemistry on target protein modification and the formation of gold-sulfur bond are confirmed. Second, the plasma converted AuNPs biosensor demonstrates the larger effective surface area and higher degree of roughness, which advances the conductivity and detection sensitivity through a higher biomolecule accessibility.

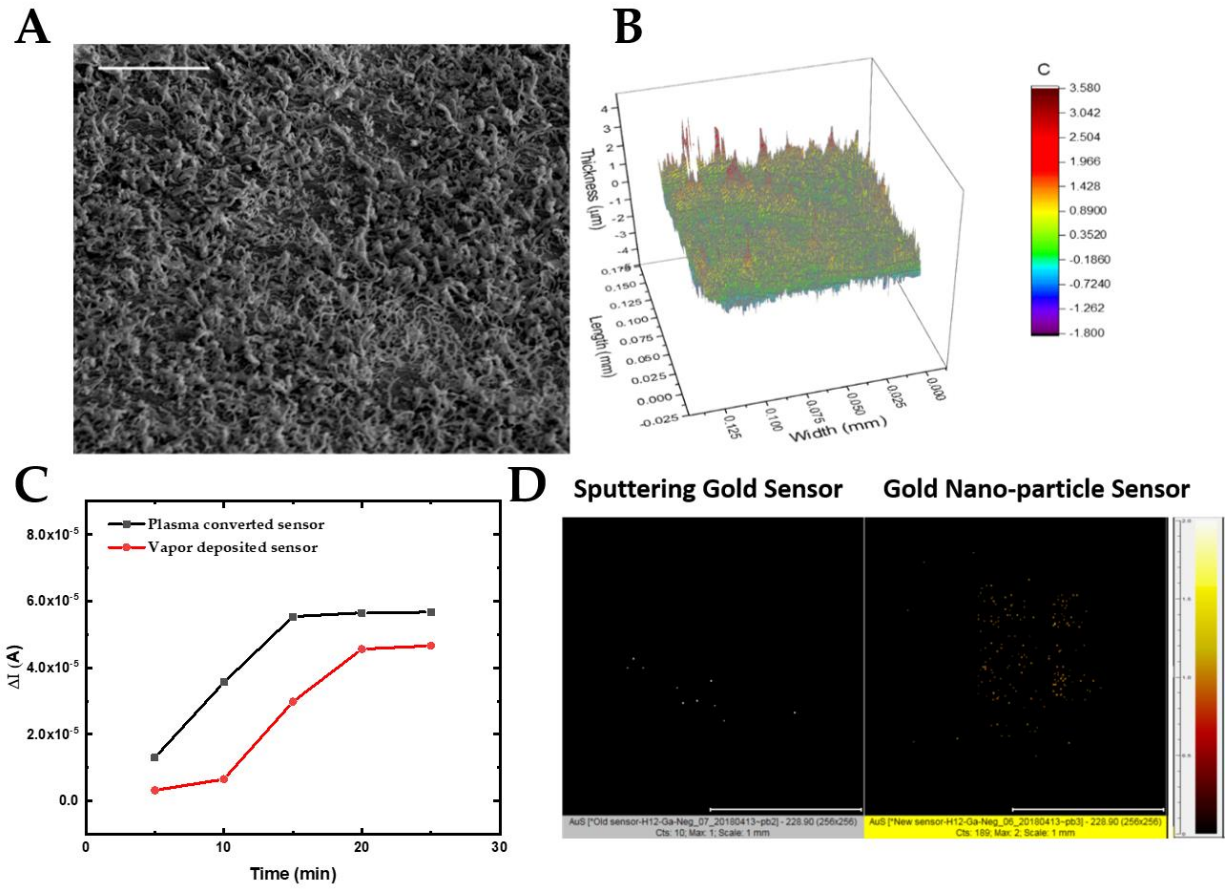

Figure 2. A) SEM top-down image of the printed AuNPs, the scale bar on the image is 10µm. B) Optical profilometry of the printed AuNPs. C) DPV examinations of biomolecule accessibility based on two different surface morphology. D) TOF-SIMS mapping of Au-S bond on the sputtering gold sensor surface and AuNPs sensor surface.

2.4 Kinetic binding model derivation

In addition to a high-sensitivity biosensor platform, an accurate mathematical model is also pivotal in order to provide accurate quantification of biomolecule interaction based on the electrochemical quantification results. Based on the current measurements from DPV as a function of the nucleic acid concentration, a steady-state binding curve was constructed using the current response ($\Delta I = I(\text{no analyte}) - I(\text{with anaylte})$) from the differential pulse voltammetry against different nucleic acid concentrations. The dissociation constant (K_D) was derived from the steady-state binding curve based on 30min of noncompetitive binding model given by Langmuir isotherm equation as shown in equation E. 1[10],

$$\Delta I = \frac{V_{max}[analyte]}{K_D + [analyte]} \qquad \text{(E. 1)}$$

in which V_{max} is the maximum reaction rate that is observed at the saturating concentration of analyte and K_D is the dissociation constant of the binding activity that is further used to calculate the off-rate (k_{off}) using the equation E. 2,

$$K_D = k_{off}/k_{on} \qquad \text{(E. 2)}$$

in which k_{on} is the on-rate/association rate that is derived from the association kinetic model through an unsteady-state condition of the following kinetic model.

The kinetic model applied in this study was derived from the traditional two compartment model, in which both transport kinetics and reaction kinetics were incorporated. Traditional kinetic analytical techniques, such as surface plasmon resonance (SPR), required complex experimental arrangements limiting the simplification of the two-compartment model[29]. However, our bio-sensing platform applied static incubation, which simplified the two-compartment model to a simple reaction kinetics model for describing the association kinetics of protein and nucleic acid. Thus, the net reaction rates of the association reaction can be derived from the following equation[6]:

$$\frac{dn}{dt} = k_m(C_b - C_s) - k_{on}C_sP + k_{off}n \quad \text{(E. 3)}$$

where k_m is the diffusion-limiting rate constant, C_b is the bulk solution concentration of the analyte nucleic acid solution, C_s is the surface concentration of the nucleic acid solution, P is the binding protein concentration on the biosensor surface, k_{on} and k_{off} are the association rate (on-rate) and dissociation rate (off-rate) describing the protein-nucleic acid binding process, and n is the concentration of protein-nucleic acid complexes on the biosensor electrode surface after protein-nucleic binding.

Unlike SPR or any flow system, the mass transport coefficient, k_m, does not contribute or affect the kinetic binding process of nucleic acid and protein in our static incubation system, minimizing the estimation error produced by any flow system kinetic modeling[30] [31]. As shown in Figure 5, the dissociation rate (off-rate) was negligible based on the time scale of binding reaction up to its saturation (which was less than 30 min). Concentrations of nucleic acid in each compartment were considered as uniform at t=0. Due to the small incubation volume of 20μL for the nucleic acid solution, the surface concentration of nucleic acid solution was assumed to be the same as the bulk concentration. When the association binding took place, the P value in the model would start decreasing with the increasing of protein-nucleic acid complexes. The amount of decreasing protein sites would equal $P - n$. Therefore, equation SI E.3 for calculating the association rate (on-rate) was expressed as E.4:

$$\frac{dn}{dt} = k_{on}(C_b)(P - n) \quad \text{(E. 4)}$$

After solving the derivative from E.4, at the condition in which C_b is the limiting reactant compared to the surface protein concentration, the integrated E.4 transformed to equation E. 5:

$$\mathrm{n(t)} = C_b - ae^{-k_aC_bt} \quad \text{(E. 5)}$$

which is the same model as the Langmuir adsorption equation and a is a constant in E. 5.

2.5 Characterization of unwinding protein 1 with SL3^{ESS3} RNA

Following the preparation of protein probe-functionalized electrode surface, quantification of interactions with different target biomolecules was carried out by electrochemical measurements using differential pulse voltammetry (DPV), which has been widely applied as a sensitive electrochemical transduction method[32-35]. The derived kinetic models in section 2.4 were applied using the DPV results to fit and quantify the biomolecules interaction. In order to establish and verify this methodology, we studied the binding behaviors between unwinding protein 1 (UP1) with SL3^{ESS3} RNA, which was examined previously by high-throughput sequencing analysis of equilibrium binding (HTS-EQ), isothermal titration calorimetry (ITC) and biolayer interferometry (BLI).[11]

Different concentrations of $SL3^{ESS3\ GUAGGAG}$ RNA were tested by the UP1 based biosensor. The procedure for fabrication of UP1 based biosensor is shown in SI. Only 20μL of each RNA sample was required for analysis. Quantification of surface UP1-SL3 RNA complexes was achieved by DPV with the presence of $[Fe[CN]_6]^{3-/4-}$requiring less than 30s for each data point. As shown in Figure 3A, the highest current output (red line) represents 0nM of $ESS3^{GUAGGAG}$ based on the UP1 immobilized biosensor under steady-state condition. The quantity of current output difference between 0nM and different concentrations was extracted as shown in Figure 3B. ΔI of different concentrations were used to construct the Hill Equation curve to obtain the dissociation constant (n>3) as shown in Figure 3C. Based on the calibration curve in Figure 3C, kinetic analysis of binding association was achieved in a time range of 0-1200s by conducting unsteady-state experiments. Three different concentrations of $ESS3^{GUAGGAG}$ were evaluated using the same concentration UP1 prepared biosensor. The dissociation constant and association rate constant obtained by electrochemical method were shown in the Figure 3C and 3D, respectively, and $K_D=6.2\times10^{-8}$ M and $k_{on}=43521\ M^{-1}s^{-1}$. k_{off} was calculated to be $2.70\times10^{-3}\ s^{-1}$ using equation E. 2. These values were compared with literature values acquired through ITC and BLI, as shown in Figure 3E[11]. The binding affinity values from these different methods are in the same magnitude, indicating that the surface immobilization of protein did not interfere with the binding ability of active binding site on the protein. Moreover, this comparison confirms that the electrochemical method and the derived kinetic model provide a feasible and proper mean for the quantification of binding behaviors of biomolecules.

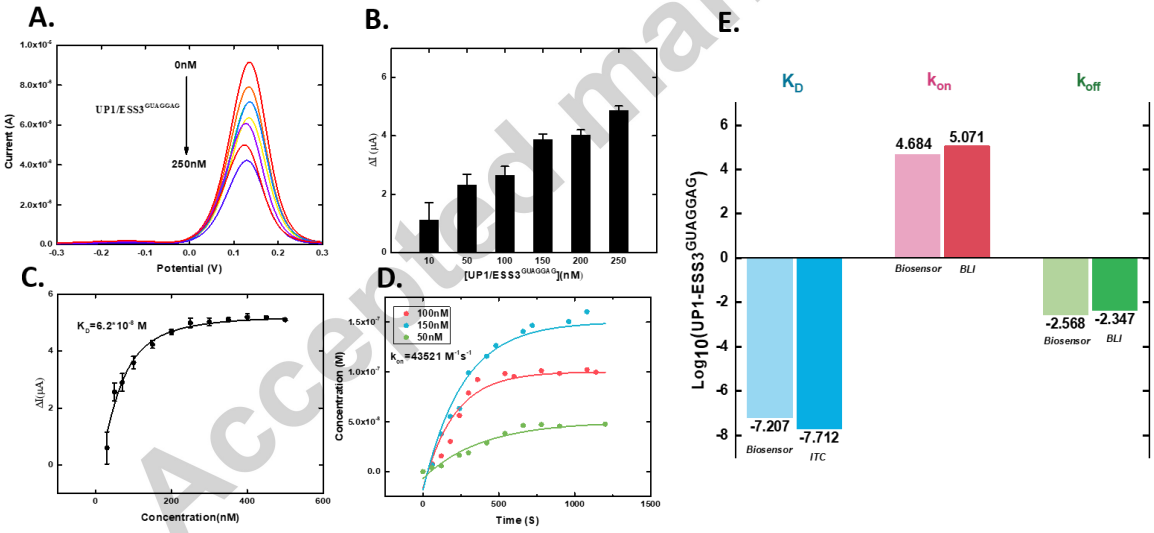

Figure 3. A) Differential pulse voltammetry quantification of $UP1/ESS3^{GUAGGAG}$ complexes on 20min interaction time. B) Different $UP1/ESS3^{GUAGGAG}$ complex concentrations against the change of current. C) Hill equation calibration curve for different concentrations of $UP1/ESS3^{GUAGGAG}$ complex against the change of current. D) Global fitting of kinetic binding curve constructed by E.5 for three different concentrations of $UP1/ESS3^{GUAGGAG}$ complex. E) Comparison of literature values of dissociation constant, association constant and off-rate constant with those values obtained from electrochemical biosensor platform.

2.6 Profiling interactions between heterogeneous nuclear ribonucleoprotein H1 with multiple DNA strands

After verification of the experimental principle, we profiled the interaction of four different DNA strands with heterogeneous nuclear ribonucleoprotein (hnRNP) H1. hnRNP H family protein plays an important role on the HIV alternative spicing and specifically recognizes G-tract nucleic acid through three consecutive guanines[9, 36]. Furthermore, G-tract nucleic acid is strongly related to the formation of triplex or quadruplex G-tract nucleic acid. Triplex and quadruplex nucleic acids have been identified negatively affecting cellular DNA replication and transcription. Therefore further impact biological processes including gene rearrangements and telomere defects can lead to human diseases, such as neuro-degenerative disorders[37, 38],[39] and various cancers[40].Thus, a rapid, simple quantification of G-tract nucleic acid using its specific binding protein is a promising method for disease control. Also, there is no detail nucleic acid binding affinity study of hnRNP H1. Also, limited information is known about the binding interactions between the sequences other than the G tract and the hnRNP H family. Thus, the characterization of the binding affinity of hnRNP H1 and the test detection accuracy and range of the electrochemical biosensor platform are of interest by comparing the ITC result.

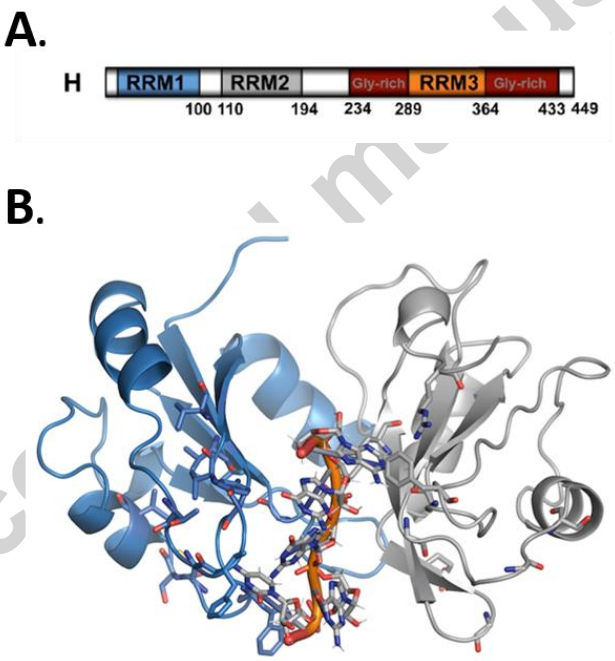

Figure 4. A) Domain organization of human hnRNP H1 showing the three RNA recognition motifs (RRM1 = blue, RRM2 = gray and RRM3 = orange) and the C-terminal glycine-rich domains (red). HqRRM12 domain boundaries used in the studies is from 10-194 residue number, including the first and second RRM domain. B) a cartoon representative HADDOCK model of the HqRRM12-AGGGC complex with showing residues involving binding.

Human hnRNP H1 consists of three quasi-RNA Recognition Motifs (qRRMs) and two glycine-rich domains (Figure 4A). At its N-terminus, qRRM1 and qRRM2, which are connected through an ~10 amino acid linker (qRRM12), whereas qRRM3 is embedded between the glycine-rich domains at its C-

terminus as shown in Figure 4B. In order to quantitatively determine the nucleic acid sequence contribution to hnRNP H1-HIV recognition, prepared hnRNP H1 biosensor (procedures shown in SI) was used to quantify different nucleic acid oligonucleotides, 5′-AAAAA-3′, 5′-AGGGG-3′, 5′-AGGGA-3′ and 5′-AGGGC-3′ (purification procedures are shown in SI). After incubation of different nucleic acid strands for 30min at room temperature, the biosensor was tested by DPV at the presence of $[Fe(CN)_6]^{3-/4-}$ to quantify the DNA-protein complexes. With a fixed amount of hnRNP H1 protein linked to the biosensor surface, the electrical impedance difference was caused by the concentration difference of the nucleic acids bonded with the target protein on the biosensor surface. The change of current comparing with the base line was plotted against different concentrations as shown in Figure 5 (upper part). The DPV detection demonstrated a reproducible result based on n>3 with an average R-square of 0.936 and RSD of 3.66%. From the Figure 5D, the poly-A region did not contribute to binding affinity since different concentrations of AAAAA displayed very minor current, while obvious difference in change of current was observed for different G-tract contained nucleic acids as shown in Figure 5A(AGGGG), 5B(AGGGC), 5C(AGGGA). Based on the quantification results from DPV, to further define and differentiate the minor difference based on G-tract DNA sequence, we applied the constructed binding affinity model and its relative curve based on multiple concentrations of DNA analyte was calibrated using E. 1. The dissociation constant (K_D) was obtained as shown in Figure 5(lower part). The data of 5′-AGGGG-3′, 5′-AGGGA-3′and 5′-AGGGC-3′ showed that hnRNP H1 binds AGGGA and AGGGC oligonucleotides with moderate affinities (K_D= 1.621-4.566 μM) and it binds strongest to 5′-AGGGG-3′ (K_D=1.308μM). In order to verify the results and compare the accuracy of our biosensing system with a standardized system, isothermal titration calorimetry (ITC) was used to test the same protein-DNA interaction. The ITC data is shown in Figure S1, and the relative binding affinity plot between ITC and biosensor is shown in Figure 6A.

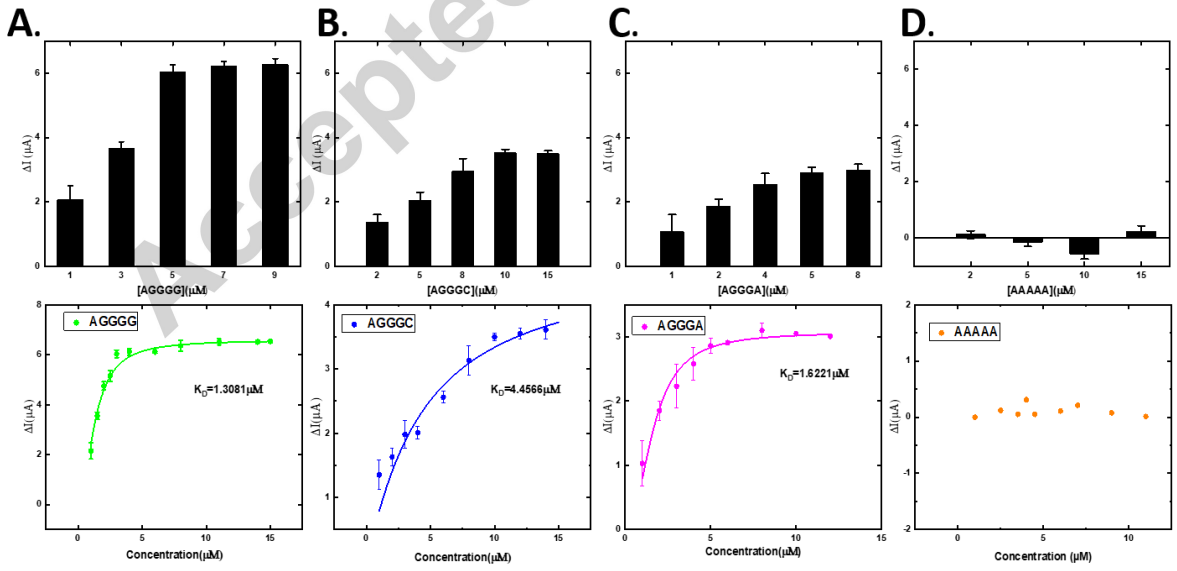

Figure 5. DPV characterization results for quantification of the complexes concentrations of different DNA strands A) AGGGG, B) AGGGA, C) AGGGC, D) AAAAA with hnRNP H1 after 30min incubation based on change of current against different concentrations of DNA-protein complexes (upper part). Hill equation fitted curves for AGGGG

(K_D=1.3081μM), AGGGC (K_D=4.4566μM), AGGGA (K_D=1.6221μM) and AAAAA (K_D=NA) based on change of current against concentrations (lower part).

We further evaluated the kinetic association rate constant of DNA-protein interaction. Unsteady-state experiment was conducted to construct a kinetic model of surface biomolecules complex concentration against time at the same concentration of nucleic acid analyte. For the same concentration of DNA analyte, a time frame of 0-1200s was applied for evaluation. Each current output data was transformed by the calibration equation constructed in Figure 5 to the value of DNA-protein complex concentrations. A non-linear global fitting of DNA-protein complex concentrations against time was conducted by kinetic equation (E. 5) to acquire the association rate, k_{on}. The association rate of AGGGG, AGGGA, AGGGC with hnRNP interaction is shown in Figure 6B, 6C, &6D. AGGGG/hnRNP H1 showed the highest rate constant, indicating the strongest binding interaction between AGGGG with hnRNP H1. The intensity sequence of the protein-nucliec acid interaction on association process was the same as the sequence of the dissociation constant derived from Hill equation in Figure 5. The results revealed general rules for specificity of hnRNP H1 providing a quantitative understanding on the discrimination between alternative competing nucleic acid ligands *in vitro*. The ability to discriminate minor binding affinity between single nucleotide differences also demonstrated the high-sensitivity performance of our biosensing platform.

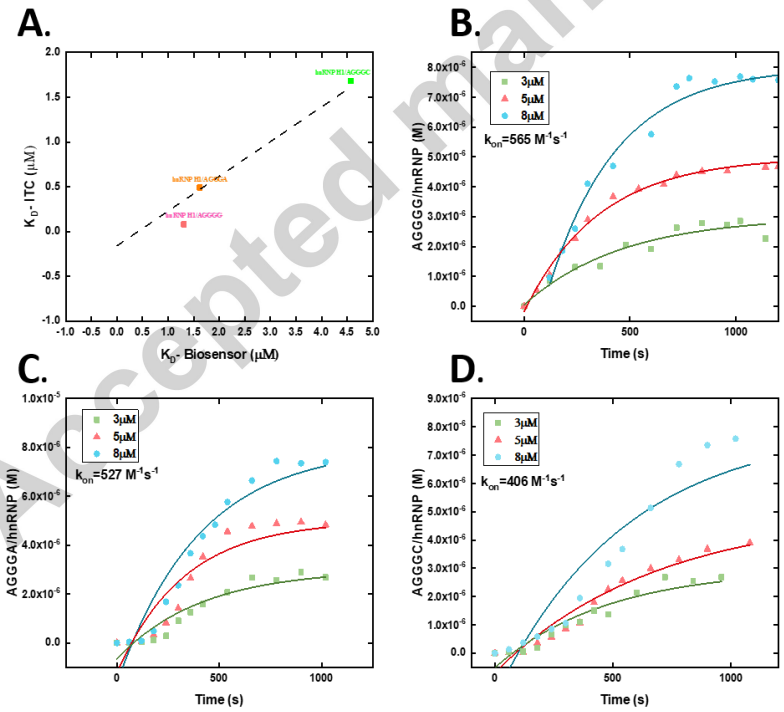

Figure 6. A) Comparison of relative binding affinities between ITC and biosensor platform. B),C),D) Association rate constant fitting for AGGGG, AGGGA, AGGGC interaction with hnRNP H1 based on complexes concentration against time in a range of 0-1200s.

In conclusion, we have developed a high-sensitivity, non-invasive biosensor platform that used plasma reduced AuNPs combined with bioconjugation chemistry for biosensor fabrication. The high-sensitivity property enabled the biosensor system to discriminate minor structure difference of G-tract nucleic acids. The quantification of G-tract nucleic acids using specific nucleic acid binding protein provides a new perspective for nucleic acids quantification using electrochemical method. Also, the binding interaction of hnRNP H1 and relative nucleic acids revealed by biosensor platform offer a quantitative aspect for hnRNP H1 differentiating between G-tract nucleic acids. This biosensor platform demonstrates a high-sensitivity method for quantification of biomolecules and analysis of binding interactions within a short analyzing timeframe and a small quantity of sample. This platform is highly versatile allowing investigation of other biomolecules interactions based on a simple, rapid and accurate quantification method.

3. Experimental

3.1 Gold nanoparticle (AuNPs) Sensor Fabrication

Ink formation and inkjet printing: 0.5 M gold (III) chloride trihydrate ($HAuCl_4 \cdot 3H_2O$, 99.9% purity, Alfa Aesar) was rendered to an ink by dissolving it in a mixture of deionized (DI) water and ethylene glycol of a 1:1 ratio. The ink was loaded into a Fujifilm Dimatix DMC-11610 material cartridge by a syringe with a 200 nm filter filtering out any particle contaminant. The inkjet printing was accomplished with a Fujifilm Dimatix DMP-3000 printer with 16 piezoelectric nozzles The spacing of the ink drops was adjusted to 15 μm and the number of printed layers was set to 3. The printing plate was heated to 50°C. Typically, an array of twenty sensors was prepared for printing at once. Prior to inkjet printing, the three-electrode based sensor prototypes were first cleaned by ethanol, followed by DI water then dried by compressed air. The cleaned sensor prototypes were placed onto the printing plate and located by a printing fiducial camera. A size of 1 mm × 1 mm square pattern of Au ink was printed on the working electrodes of the sensor prototype.

Plasma treatment: Plasma treatment was performed in a pure argon (Purity 99.9999%, Air Gas) environment. The plasma chamber (March PX250) was connected to an external 600 W, 13.56 MHz RF power supply (ENI, ACE-6B-06). The sensors with inkjet-printed Au electrodes were placed on the power plate of the capacitive coupled plasma system. The chamber was evacuated to 60 mTorr and then purged with Ar for 10 minutes ensuring the absence of any foreign species. Plasma treatment of the printed gold nanoparticle film was carried out at 300 W plasma power and 600 mTorr background pressure for 15 minutes.

3.2 Differential pulse voltammetry evaluations of biomolecules complexes

Differential pulse voltammetry was used as the electrochemical transduction mechanism for biomolecular quantification. Firstly, biosensors immobilized with unwinding protein 1(UP1) were tested with HIV ESS3 RNA demonstrating the validity of the electrochemical method based quantification model. Secondly, for the purpose of determining the interaction between hnRNP H1 protein and different DNA, a hnRNP H1 protein immobilized biosensor was used to quantify the amount of DNA-protein complexes formed on the biosensor surface. Purified DNA sequences were diluted by a 0.1M PBS solution into different concentrations. 20μL of diluted DNA solution was drop-casted onto the biosensor with a static incubation time of 30 min. After incubation, the biosensors were rinsed by 0.1M PBS solution and dried by nitrogen gas before electrochemical testing. For differential pulse voltammetry, a potential range of -0.3 V to +0.3 V (versus the Ag/AgCl reference electrode) was applied with a potential increment of 0.004V, an amplitude of 0.05V, a pulse width of 0.05s, a sampling width of 0.0167s and a pulse period

of 0.2s. 20μL of redox coupling solution, $K_3Fe(CN)_6$ and $K_4Fe(CN)_6$, with 5mM in each component was dropped onto the biosensor immediately prior to DPV measurement, which took around 30s to complete.

3.3 Differential pulse voltammetry for unsteady-state analysis of kinetic binding behavior

For biomolecules binding kinetic analysis, an array of ten bioconjugation chemistry prepared hnRNP H1 biosensors were employed. A time range of 0-1200s for incubation time was applied for the kinetic analysis. 20μL each biosensor of certain concentration of the specific DNA strand (such as AGGGG) was dropped cast onto all the prepared biosensors. Before individual testing, the tested biosensor was rinsed by DI water and dried by nitrogen gas. At the beginning of the kinetic experiment, 45-100s interval per test was conducted by DPV to obtain the build-up process of the kinetic; after the significant change of current was observed, 100-300s interval per test was conducted to study the saturation of the binding association behavior. Once the saturation behavior was confirmed by three consecutive stable current output, the whole association kinetic test was considered complete.

Acknowledgements

The research reported in this publication was partially supported by National Institute of Health award (Grant #1 S10 RR025660-01A1). Portion of this research were supported by National Institute of Health award (Grant #R01GM101979) and National Science Foundation (CMMI-1246715) and were also greatly appreciated and acknowledged. We acknowledge the help from Ohio State University: Mass Spectrometry and Proteomics Facility and Case Western Reserve University: Swagelok Center for Surface Analysis of Materials. We also acknowledge the use of facilities of Electronics Design Center of Case Western Reserve University.

Conflict of Interest

The authors declare no conflict of interest.

References

[1] T. Raub, C. Barsuhn, L. Williams, D. Decker, G. Sawada, N. Ho, Use of a biophysical-kinetic model to understand the roles of protein binding and membrane partitioning on passive diffusion of highly lipophilic molecules across cellular barriers, Journal of drug targeting 1(4) (1993) 269-286.

[2] P. Schuck, H. Zhao, The role of mass transport limitation and surface heterogeneity in the biophysical characterization of macromolecular binding processes by SPR biosensing, Surface plasmon resonance, Springer2010, pp. 15-54.
[3] N. Soh, T. Tokuda, T. Watanabe, K. Mishima, T. Imato, T. Masadome, Y. Asano, S. Okutani, O. Niwa, S. Brown, A surface plasmon resonance immunosensor for detecting a dioxin precursor using a gold binding polypeptide, Talanta 60(4) (2003) 733-745.
[4] X. Duan, Y. Li, N.K. Rajan, D.A. Routenberg, Y. Modis, M.A. Reed, Quantification of the affinities and kinetics of protein interactions using silicon nanowire biosensors, Nature nanotechnology 7(6) (2012) 401.
[5] Q. Feng, N.-Q. Li, Y.-Y. Jiang, Electrochemical studies of porphyrin interacting with DNA and determination of DNA, Analytica Chimica Acta 344(1-2) (1997) 97-104.
[6] R.S. Gaster, L. Xu, S.-J. Han, R.J. Wilson, D.A. Hall, S.J. Osterfeld, H. Yu, S.X. Wang, Quantification of protein interactions and solution transport using high-density GMR sensor arrays, Nature nanotechnology 6(5) (2011) 314.
[7] Y. Dai, A. Molazemhosseini, C.C. Liu, A Single-Use, In Vitro Biosensor for the Detection of T-Tau Protein, A Biomarker of Neuro-Degenerative Disorders, in PBS and Human Serum Using Differential Pulse Voltammetry (DPV), Biosensors 7(1) (2017) 10.
[8] L.-Y. Chiu, K.-W. Hung, S.-C. Tjong, Y.-W. Chiang, S.-C. Sue, NMR characterization of the electrostatic interaction of the basic residues in HDGF and FGF2 during heparin binding, Biochimica et Biophysica Acta (BBA)-Proteins and Proteomics 1844(10) (2014) 1851-1859.
[9] C. Dominguez, J.-F. Fisette, B. Chabot, F.H. Allain, Structural basis of G-tract recognition and encaging by hnRNP F quasi-RRMs, Nature Structural and Molecular Biology 17(7) (2010) 853.
[10] C.E. Morgan, J.L. Meagher, J.D. Levengood, J. Delproposto, C. Rollins, J.A. Stuckey, B.S. Tolbert, The first crystal structure of the UP1 domain of hnRNP A1 bound to RNA reveals a new look for an old RNA binding protein, Journal of molecular biology 427(20) (2015) 3241-3257.
[11] N. Jain, H.-C. Lin, C.E. Morgan, M.E. Harris, B.S. Tolbert, Rules of RNA specificity of hnRNP A1 revealed by global and quantitative analysis of its affinity distribution, Proceedings of the National Academy of Sciences (2017) 201616371.
[12] L. Soleymani, Z. Fang, E.H. Sargent, S.O. Kelley, Programming the detection limits of biosensors through controlled nanostructuring, Nature Nanotechnology 4(12) (2009) 844.
[13] J.M. Pingarrón, P. Yanez-Sedeno, A. González-Cortés, Gold nanoparticle-based electrochemical biosensors, Electrochimica Acta 53(19) (2008) 5848-5866.
[14] V.R. Marinov, Y.A. Atanasov, A. Khan, D. Vaselaar, A. Halvorsen, D.L. Schulz, D.B. Chrisey, Direct-write vapor sensors on FR4 plastic substrates, IEEE Sensors Journal 7(6) (2007) 937-944.
[15] J.C. Love, L.A. Estroff, J.K. Kriebel, R.G. Nuzzo, G.M. Whitesides, Self-assembled monolayers of thiolates on metals as a form of nanotechnology, Chemical reviews 105(4) (2005) 1103-1170.
[16] C. Vericat, M. Vela, G. Benitez, P. Carro, R. Salvarezza, Self-assembled monolayers of thiols and dithiols on gold: new challenges for a well-known system, Chemical Society Reviews 39(5) (2010) 1805-1834.
[17] K. Bonroy, F. Frederix, G. Reekmans, E. Dewolf, R. De Palma, G. Borghs, P. Declerck, B. Goddeeris, Comparison of random and oriented immobilisation of antibody fragments on mixed self-assembled monolayers, Journal of immunological methods 312(1) (2006) 167-181.
[18] S.K. Vashist, Comparison of 1-ethyl-3-(3-dimethylaminopropyl) carbodiimide based strategies to crosslink antibodies on amine-functionalized platforms for immunodiagnostic applications, Diagnostics 2(3) (2012) 23-33.
[19] J.W. Lee, S.J. Sim, S.M. Cho, J. Lee, Characterization of a self-assembled monolayer of thiol on a gold surface and the fabrication of a biosensor chip based on surface plasmon resonance for detecting anti-GAD antibody, Biosensors and Bioelectronics 20(7) (2005) 1422-1427.

[20] Y. Dai, C. Wang, L.-Y. Chiu, K. Abbasi, B.S. Tolbert, G. Sauvé, Y. Yen, C.-C. Liu, Application of Bioconjugation Chemistry on Biosensor Fabrication for Detection of TAR-DNA binding Protein 43, Biosensors and Bioelectronics.
[21] S.O. Kelley, C.A. Mirkin, D.R. Walt, R.F. Ismagilov, M. Toner, E.H. Sargent, Advancing the speed, sensitivity and accuracy of biomolecular detection using multi-length-scale engineering, Nature nanotechnology 9(12) (2014) 969.
[22] M. Labib, R.M. Mohamadi, M. Poudineh, S.U. Ahmed, I. Ivanov, C.-L. Huang, M. Moosavi, E.H. Sargent, S.O. Kelley, Single-cell mRNA cytometry via sequence-specific nanoparticle clustering and trapping, Nature chemistry (2018) 1.
[23] A.A.I. Sina, S. Howell, L.G. Carrascosa, S. Rauf, M.J. Shiddiky, M. Trau, eMethylsorb: electrochemical quantification of DNA methylation at CpG resolution using DNA–gold affinity interactions, Chemical Communications 50(86) (2014) 13153-13156.
[24] K.M. Koo, L.G. Carrascosa, M.J. Shiddiky, M. Trau, Poly (A) extensions of miRNAs for amplification-free electrochemical detection on screen-printed gold electrodes, Analytical chemistry 88(4) (2016) 2000-2005.
[25] J.N. Weiss, The Hill equation revisited: uses and misuses, The FASEB Journal 11(11) (1997) 835-841.
[26] Y. Dai, C. Wang, L.-Y. Chiu, K. Abbasi, B.S. Tolbert, G. Sauvé, Y. Yen, C.-C. Liu, Application of bioconjugation chemistry on biosensor fabrication for detection of TAR-DNA binding protein 43, Biosensors and Bioelectronics 117 (2018) 60-67.
[27] V.F. Lvovich, Impedance spectroscopy: applications to electrochemical and dielectric phenomena, John Wiley & Sons2012.
[28] C. Richmonds, R.M. Sankaran, Plasma-liquid electrochemistry: rapid synthesis of colloidal metal nanoparticles by microplasma reduction of aqueous cations, Applied Physics Letters 93(13) (2008) 131501.
[29] S.G. Patching, Surface plasmon resonance spectroscopy for characterisation of membrane protein–ligand interactions and its potential for drug discovery, Biochimica et Biophysica Acta (BBA)-Biomembranes 1838(1) (2014) 43-55.
[30] C. Hahnefeld, S. Drewianka, F.W. Herberg, Determination of kinetic data using surface plasmon resonance biosensors, Molecular diagnosis of infectious diseases, Springer2004, pp. 299-320.
[31] D.G. Myszka, Kinetic analysis of macromolecular interactions using surface plasmon resonance biosensors, Current opinion in biotechnology 8(1) (1997) 50-57.
[32] Y. Dai, C.C. Liu, A Simple, Cost-Effective Sensor for Detecting Lead Ions in Water Using Under-Potential Deposited Bismuth Sub-Layer with Differential Pulse Voltammetry (DPV), Sensors 17(5) (2017) 950.
[33] Y. Dai, C. chiun Liu, Detection of 17 β-estradiol in Environmental Estrogen Pollution and in Women's Health Care Using a Single-Use, Cost Effective Biosensor Based on Differential Pulse Voltammetry (DPV), (2017).
[34] B. Shui, D. Tao, J. Cheng, Y. Mei, N. Jaffrezic-Renault, Z. Guo, A novel electrochemical aptamer–antibody sandwich assay for the detection of tau-381 in human serum, Analyst 143(15) (2018) 3549-3554.
[35] Y. Dai, K. Abbasi, M. DePietro, S. Butler, C.C. Liu, Advanced fabrication of biosensor on detection of Glypican-1 using S-Acetylmercaptosuccinic anhydride (SAMSA) modification of antibody, Scientific Reports 8(1) (2018) 13541.
[36] S.R. Penumutchu, L.-Y. Chiu, J.L. Meagher, A.L. Hansen, J.A. Stuckey, B.S. Tolbert, Differential Conformational Dynamics Encoded by the Linker between Quasi RNA Recognition Motifs of Heterogeneous Nuclear Ribonucleoprotein H, Journal of the American Chemical Society 140(37) (2018) 11661-11673.

[37] N.A. Di Prospero, K.H. Fischbeck, Therapeutics development for triplet repeat expansion diseases, Nature Reviews Genetics 6(10) (2005) 756.
[38] Y. Wu, R.M. Brosh, G‐quadruplex nucleic acids and human disease, The FEBS journal 277(17) (2010) 3470-3488.
[39] D.C. Crawford, J.M. Acuña, S.L. Sherman, FMR1 and the fragile X syndrome: human genome epidemiology review, Genetics in Medicine 3(5) (2001) 359.
[40] P.M. Lansdorp, Telomeres and disease, The EMBO journal 28(17) (2009) 2532-2540.

Highlights

- Simple, rapid, and accurate general electrochemical method for biomolecules binding affinity analysis.
- Plasma produced gold nanoparticle sensor.
- Detail analysis of G-tract nucleic acids interaction with heterogeneous nuclear ribonucleoprotein H1 (hnRNP H1).